OM&P

Differential Contribution of GLAST and GLT-1 to Network Sodium Signaling in the Early Postnatal Hippocampus

*Claudia Karus, Niklas J. Gerkau & Christine R. Rose**

Institute of Neurobiology, Faculty of Mathematics and Natural Sciences, Heinrich Heine University Düsseldorf, Universitätsstrasse 1, D-40225 Düsseldorf, Germany.
* Corresponding e-mail: rose@hhu.de

Abstract. Recurrent epileptiform activity induces network sodium oscillations in the juvenile hippocampus. In CA1 pyramidal neurons, these oscillations are mainly caused by opening of glutamate-gated ion channels, while in astrocytes, sodium increases are due to sodium-dependent glutamate uptake. Astrocytes express the glutamate transporters GLAST and GLT- 1, which exhibit differential expression patterns during postnatal development. The specific contribution of these transporter subtypes to sodium oscillations is not known. We addressed this question by performing somatic sodium imaging in hippocampal tissue slices from neonatal (postnatal days (P) 2-4) and two-week-old (P14-16) mice. We found that perfusion with Mg^{2+}-free, bicuculline-containing saline caused sodium oscillations in both developmental stages. Moreover, at both P2-4 and P14-16, application of TFB-TBOA to inhibit GLAST and GLT-1 generated fast sodium loading of neurons and termination of oscillatory activity, accompanied by loss of membrane integrity of neurons, while astrocytes experienced only minor increases in baseline sodium. DHK, a GLT-1-specific blocker, induced moderate sodium loading of neurons, reduced the amplitude of neuronal sodium oscillations and increased the oscillation frequency in two-week-old mice. In neonatal animals, DHK increased baseline sodium and reduced the peak amplitude of sodium transients as well, but exerted only moderate effects on network activity. Taken together, our experiments demonstrate the essential role of glutamate uptake for sodium homeostasis and neural function already in the early neonatal brain. Moreover, they suggest that, although GLAST dominates in neonatal tissue and GLT-1 is predominant at P14-16, both transporter subtypes functionally contribute to glutamate clearance during the first three weeks after birth.

Keywords: glutamate uptake, astrocyte, pyramidal neuron, glia, SBFI

Introduction

It is well established that astrocytes communicate with each other by intra- and intercellular calcium signals, which are also of importance for their interaction with neurons (Attwell et al., 2010; Nedergaard et al., 2012; Araque et al., 2014; Rusakov, 2015). In addition, astrocytes can be subject to transient activity-related increases in their sodium concentration, which can either be confined to processes or invade the somata depending on the strength of stimulation (Kirischuk et al., 2012; Rose et al., 2013). Sodium signaling can even include the entire population of astrocytes in a given brain region, as demonstrated upon pharmacological induction of recurrent network activity in tissue slices of the mouse hippocampus (Karus et al., 2015a). The latter study moreover showed that sodium signaling in the dis-inhibited hippocampus also comprises CA1 pyramidal neurons, oscillating parallel to the electrical activity. Interestingly, metabolic integrity of astrocytes was required for the neurons' capacity to maintain low sodium levels and to recover from sodium loads accompanying network oscillations, demonstrating an intimate metabolic coupling between the two cell types. Moreover, addition of lactate supported neuronal - but not glial - sodium homeostasis and largely reversed the effects of glial poisoning by the metabolic inhibitor sodium-fluoroacetate (Karus et al., 2015b; Gerkau et al., 2017).

While their specific involvement in intracellular signaling is still unclear (Rose et al., 2016b), activity-related increases in astrocyte sodium are known to serve an important role in astrocyte metabolism and neuro-metabolic coupling (Pellerin et al., 2012; Chatton et al., 2016; Rose et al., 2016a). Evidently, elevation of intracellular sodium directly alters the activity of sodium-dependent transporters (Rose et al., 2013; Rose et al., 2016c) and may thereby e.g. result in reversal of the sodium/calcium exchanger (NCX) and in calcium influx (Parpura et al., 2016). Increases in astrocyte sodium also promote the release of glutamine, driving the glutamate-glutamine shuttle (Bak et al., 2006; Uwechue et al., 2012) and may cause reversal of GABA uptake and furthermore the release of GABA from astrocytes (Kirischuk et al., 2016). Additionally, intracellular sodium elevations are central to excitotoxic damage and critically involved in the dysfunction and injury of both neurons and astrocytes in neurodegenerative disease (Somjen, 2002; Boscia et al., 2016).

In the juvenile hippocampus and cerebellum, astrocyte sodium transients are mainly generated due to activation of sodium-dependent glutamate uptake (Kirischuk et al., 2007; Bennay et al., 2008; Langer et al., 2009). The uptake of glutamate is vital for the protection of brain tissue against excitotoxic damage. Indeed, in slices undergoing recurrent activity, inhibition of glutamate transporters by TFB-TBOA caused acceleration, followed by cessation of electrical activity, irreversible sodium increases and

swelling of neurons, emphasising their essential role for network activity (Karus et al., 2015a). Astrocytes mainly express two subtypes of glutamate transporters, GLT-1 (glutamate transporter-1) and GLAST (glutamate-aspartate transporter) (Danbolt, 2001; Rose et al., 2016d). Relative expression levels of these transporters change during early postnatal development (Furuta et al., 1997; Kugler et al., 2004; Schreiner et al., 2014): GLAST is the predominant subtype in neonatal brain, while GLT-1 is hardly detectable at this age. Strong upregulation of GLT-1 expression occurs during the second week after birth and GLT-1 then assumes a dominating role in the mature brain.

While the critical role of glutamate transporters for generation of astrocyte sodium signaling and the functional integrity of neurons is established, the specific involvement of GLAST versus GLT-1 in network sodium signaling at different stages of postnatal development is unclear. In the present study, we addressed this question by performing quantitative, wide-field sodium imaging with the fluorescent indicator dye SBFI in somata of neurons and astrocytes in acutely isolated tissue slices of the mouse hippocampus derived from neonate (postnatal day (P) 2-4) as well as two-week-old (P14-16) animals.

Methods

This study was carried out in accordance with the institutional guidelines of the Heinrich Heine University Duesseldorf, as well as the European Community Council Directive (86/609/EEC). All experiments were communicated to and approved by the Animal Welfare Office at the Animal Care and Use Facility of the Heinrich Heine University Duesseldorf (institutional act number: O52/05). In accordance with the German Animal Welfare Act (Tierschutzgesetz, Articles 4 and 7), no formal additional approval for the post-mortem removal of brain tissue was necessary.

Preparation of tissue slices and salines

Acute brain slices were prepared from Balb/c mice (both sexes; neonatal: postnatal days (P) 2-4; two-week-old: P14-16). In accordance with the recommendations of the European Commission (published in: Euthanasia of experimental animals, Luxembourg: Office for Official Publications of the European Communities, 1997; ISBN 92–827–9694-9), P14-16 mice were anaesthetized with CO_2 before the animals were quickly decapitated.

Following standard procedures (Edwards et al., 1989; Meier et al., 2006), hippocampal tissue slices were prepared in ice-cold modified artificial cerebrospinal fluid (mACSF) containing (in mM): 125 NaCl, 2.5 KCl, 0.5 $CaCl_2$, 6 $MgCl_2$, 1.25 NaH_2PO_4, 26 $NaHCO_3$, and 20 glucose, bubbled with 95% O_2 and 5% CO_2 to result in a pH of 7.30. Osmolarity was 310 ± 5 mOsm/l. After sectioning, slices were transferred for 20 minutes into mACSF at 34°C to which 0.5-1 µM sulforhodamine 101 (SR101) was added for selective labeling of astrocytes (Nimmerjahn et al., 2004; Kafitz et al., 2008). Slices were then kept for another 10 minutes at 34°C in ACSF (containing 2 mM $CaCl_2$ and 1 mM $MgCl_2$ but otherwise identical to mACSF), before transferring them to ACSF at room temperature (19-22°C). All experiments were performed at room temperature.

Nominally magnesium-free saline ("0 Mg^{2+}") was prepared identical to ACSF except without addition of $MgCl_2$. Pharmacological substances were applied via bath perfusion. Chemicals were purchased from Sigma-Aldrich Chemicals (Munich, Germany) except for dihydrokainate (DHK) and (2S,3S)-3-[3-[4-(trifluoromethyl)benzoylamino]-benzyloxy]aspartate (TFB-TBOA) (both Tocris Bioscience, Bristol, UK).

Sodium imaging

Cells in the hippocampal CA1 stratum pyramidale and stratum radiatum were bolus loaded with the membrane-permeable variant of SBFI (SBFI-AM: sodium-binding benzofurane isophthalate-acetoxymethyl ester; TEFlabs, Austin, Texas, USA and Invitrogen (Molecular Probes), Eugene, Oregon, USA) as previously described (Langer et al., 2009). SBFI was injected by brief focal pressure application into the tissue using glass micropipettes prepared from borosilicate capillaries (Hilgenberg) coupled to a pressure application device (PDES-02D, NPI Electronic GmbH, Tamm, Germany). Dye-loaded slices were analyzed using a wide-field epifluorescence microscope (Axioscope, Zeiss, Göttingen, Germany) equipped with a LUMPLFLN 40x objective (water immersion, N.A: 0.8, Olympus Europe, Hamburg, Germany) and employing a digital imaging system. The latter consisted of a monochromator equipped with a Xenon arch lamp (PolyV, FEI (Till Photonics), Gräfelfing, Germany) and a camera (Orca Flash 4.0, Hamamatsu Photonics K.K., Japan), controlled by NIS elements software (Nikon GmbH, Düsseldorf, Germany).

SR101 fluorescence was excited at 575 nm and collected above 590 nm, while SBFI was excited alternatingly at 340 nm (weakly sodium-sensitive) and 380 nm (sodium-sensitive wavelength), (cf. Langer et al., 2009; Karus et al., 2015a) and its fluorescence collected >420 nm. Figure 1A shows typical staining patterns obtained in the wide-field imaging system in slices from neonate (Fig. 1A1) and P14-16 (Fig. 1A2) animals, illustrating that neurons and astrocytes were clearly distinguishable based on the SR101 fluorescence. Fluorescence analysis was restricted to defined regions of interest (ROIs) representing cell somata. The ratio of 340 nm/380 nm fluorescence was calculated and analyzed offline using OriginPro 9G software (OriginLab Corporation, Northhampton, MA, USA) after a standard background correction was performed as previously described (Langer et al., 2009; Langer et al., 2012). Changes in SBFI fluorescence ratio are expressed as changes in sodium concentration based on *in situ* calibrations, performed as previously described in detail (Meier et al., 2006; Langer et al., 2009; Karus et al., 2015a).

 doi:10.20388/omp2017.003.0048

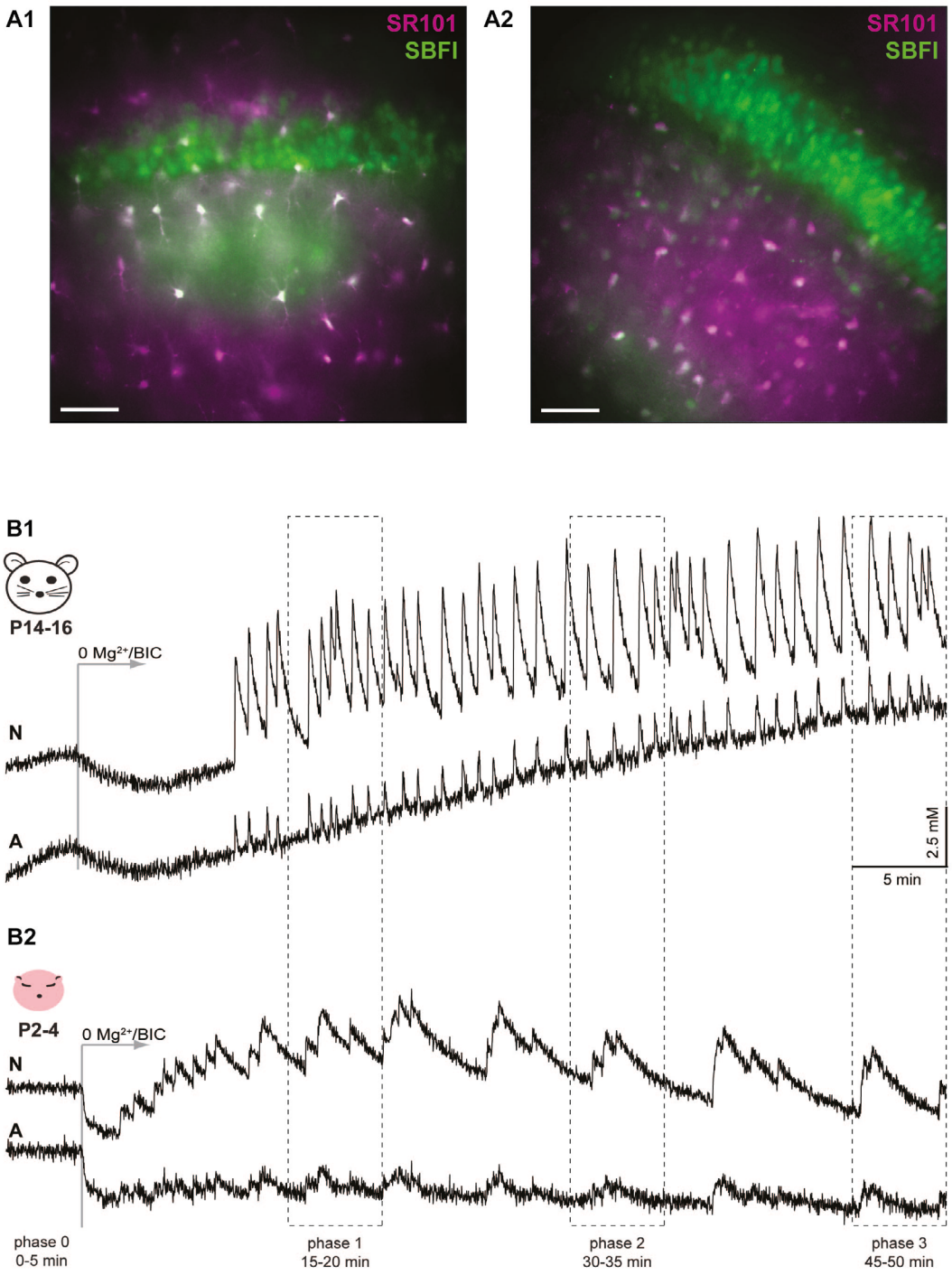

Figure 1. *Network sodium oscillations induced by dis-inhibition in early postnatal hippocampus. A) Merged epifluorescence images of the CA1 region from P14-16 (A1) and neonatal (A2) slices stained with SBFI (green) and SR101 (magenta). The scale bars indicate 50 µm. B) Application of 0Mg²⁺/BIC induced recurrent sodium oscillations in neurons (upper trace; N) and astrocytes (lower trace; A) in both P14-16 (B1) as well as neonatal (B2) tissue slices. The traces represent averages of all individual cells from the illustrated experiment. The time windows in which detailed analyses were performed (phase 0-3) are indicated.*

Analysis of cell morphology

Images were taken using a custom-built multiphoton laser-scanning microscope based on a Fluoview 300 system (Olympus Europe, Hamburg, Germany), equipped with a water immersion objective (NIR Apo 60x/NA 1.0; Nikon GmbH, Düsseldorf, Germany). For excitation, a tunable femtosecond-pulsed IR laser (MaiTai; Spectra Physics, Darmstadt, Germany) was used. Excitation wavelength was 800 nm, fluorescence emission was collected below 700 nm. Z-stacks (step size 1 µm; x-y-resolution: 0.51 µm/pixel; 2x Kalman filter) of SBFI fluorescence were taken, post-processed employing deconvolution (Huygens Professional, SVI imaging, Hilversum, Netherlands) and are illustrated as maximal intensity projection images.

Data presentation and statistics

All experiments were performed on slices obtained from at least three different animals. Unless otherwise specified, data are presented as means ± standard error of the mean and were statistically analyzed via one way ANOVA and post hoc Bonferroni test. p represents error probability, n.s. indicates if no significant difference was detected. * ≡ $p<0.05$; ** ≡ $p<0.01$; *** ≡ $p<0.001$. n represents the number of cells or individual signals as indicated, N the number of slices studied.

Results

Network sodium signaling in early postnatal hippocampus

During perfusion with standard ACSF, baseline sodium concentrations as measured in the cell bodies of neurons and astrocytes did not display detectable "spontaneous" fluctuations (Fig. 1B; cf. Figs. 4A, 5A). To study activity-related cellular sodium signaling, we employed a protocol for induction of endogenous network activity. Slices were first perfused with standard ACSF ("phase 0") and then exposed to Mg^{2+}-free saline, to which 10 µM bicuculline was added ("0Mg^{2+}/BIC") for at least 45 more minutes (Fig. 1B). This manipulation relieves the Mg^{2+}-block of NMDA receptors and prevents activation of $GABA_A$ receptors

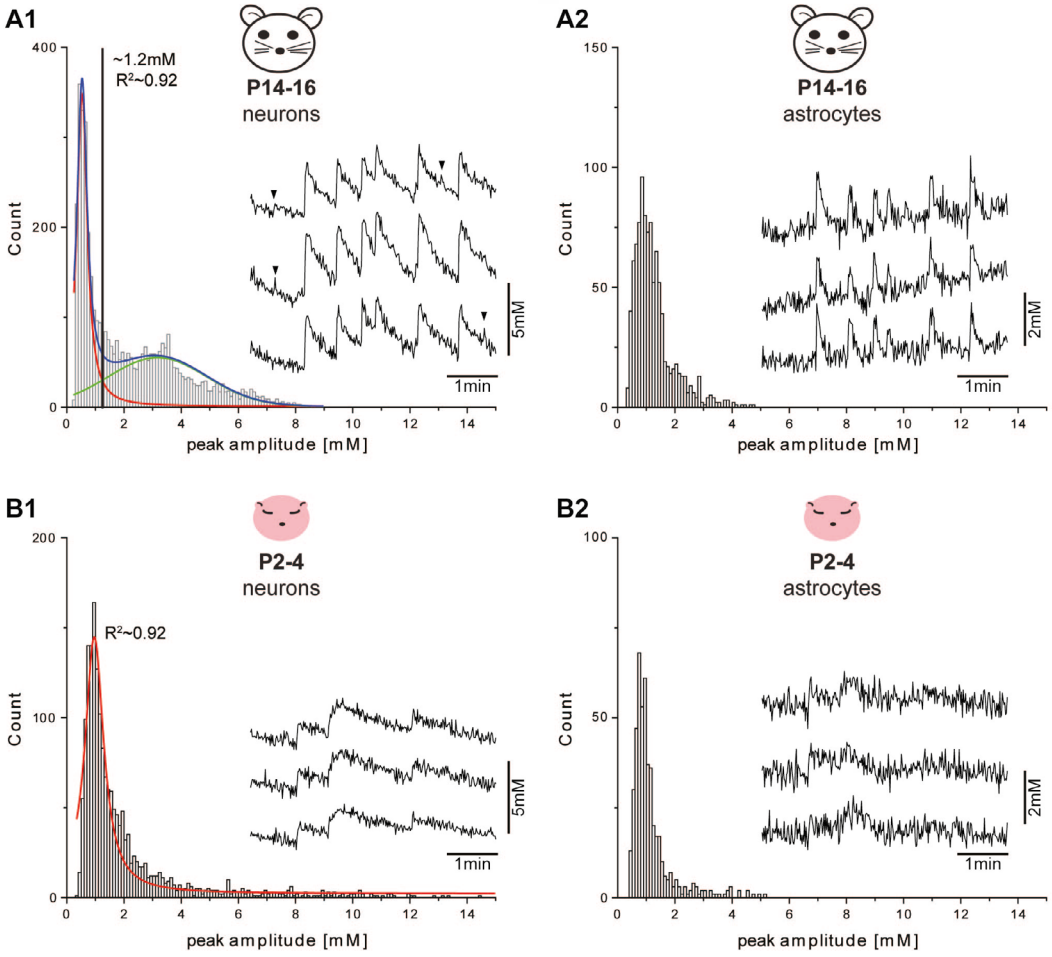

Figure 2. *Amplitude distributions of neuronal and glial sodium transients. The histogram plots show the distribution of peak sodium amplitudes (bin size 0.1 mM) taken from phase 1 of all experiments included in this study. A) depicts the results from P14-16 slices (A1: neurons; A2: astrocytes) while B shows the results for neonatal tissue (B1: neurons; B2: astrocytes). The data in A1) and B1) were fitted using a Voigt peak fit to analyze their distribution. While neonatal neuronal signals were fit best by a single distribution, sodium transients from P14-16 neurons followed a bimodal distribution as indicated by the different colors. The intersection of the fit curves (at ~1.2 mM) was set as threshold separating small from large signals. The insets show sodium oscillations of the single cells of the respective cell type. Arrowheads in A1) point to small signals.*

 doi:10.20388/omp2017.003.0048

(shown by Fellin et al., 2006; Rouach et al., 2008). It results in ongoing recurrent epileptiform bursting of neurons, transient increases in $[K^+]_o$, and concurrent astrocyte depolarizations in the juvenile mouse hippocampus (Karus et al., 2015a). Of note, and as reported earlier (Karus et al., 2015a), bicuculline absorbs light in the UV range, producing an initial, sodium-independent drop of the fluorescence ratio of SBFI during its wash-in, which results in an apparent baseline reduction by ~1-2 mM (Fig. 1B; cf. Figs. 4A, 5A).

In tissue derived from two-week-old animals (P14-16; N=10 slices), perfusion with $0Mg^{2+}$/BIC saline resulted in the generation of synchronized network sodium oscillations (Fig. 1B) at a frequency of about 2 transients per minute (Fig. 3B1), developing after about 10 minutes (586 ± 31 s) and encompassing pyramidal neurons as well as astrocytes. In accordance with our previous study (Karus et al., 2015a), neurons exhibited large amplitude signals, superimposed with small signals close to the detection threshold. In the period of 15-20 minutes after starting the experiment ("phase 1"; cf. Fig. 1B), small signals averaged 0.7 ± 0.005 mM (n=1.909 signals), while large signals amounted to 3.4 ± 0.03 mM (n=2.312 signals) (Fig. 2A1). Sodium signals in astrocytes displayed a single peak of 1.3 ± 0.02 mM (n=983 signals) and were clearly discernible only in parallel to large neuronal transients (Fig. 2A2).

In tissue derived from neonate animals (N=12), perfusion with $0Mg^{2+}$/BIC saline resulted in intracellular sodium oscillations that already started within about 3 minutes (172.0 ± 24.2 s) and exhibited a frequency of about 1 transient per minute (Fig. 1B2, 3B2). Peak amplitudes of neuronal sodium transients averaged 2.0 ± 0.05 mM (n=1781 signals) and did, in contrast to P14-16, not show a biphasic distribution (Fig. 2B1). Sodium transients in neonatal astrocytes occurred simultaneous to neuronal transients and were slightly smaller than astroglial signals in tissue derived from P14-16 animals (avg. peak amplitude 1.2 ± 0.03 mM, n=475 signals; p=0.027) (Fig. 2B2).

Oscillations were rather stable and stayed so in spite of prolonged $0Mg^{2+}$/BIC presence in both P14-16 and neonate animals. The peak amplitude of neuronal as well as astrocyte sodium oscillations was essentially unaltered during the three phases of analysis (phase 1: 15-20 minutes, phase 2: 30-35 minutes, phase 3: 45-50 minutes; cf. Fig. 1B). Minor fluctuations in the sodium signal-frequency occurred over time in P14-16 neurones, and the sodium signal-frequency decreased slightly in neonates (Fig. 3B). Alongside developing stable sodium oscillations, the apparent baseline sodium concentration of both neurons and astrocytes showed slight changes during the continued presence of $0Mg^{2+}$/BIC in P14-16 animals (N=4). In phase 3, neuronal sodium had increased by 2.7 ± 0.1 mM (n=227 cells), while astrocyte sodium had increased by 0.3 ± 0.1 mM (n=82 cells) as compared to phase 1 (Fig. 3C1). In neonates (N=5), astrocyte sodium did not change significantly (n=92 cells), and neuronal sodium dropped slightly (n=257 cells) (Fig. 3C2).

Taken together, these results confirm that dis-inhibition causes stable network sodium oscillations in both neurons and astrocytes in tissue slices of the hippocampal CA1 region derived from two-week-old mice. Moreover, our experiments show that this phenomenon is also present in tissue derived from early neonatal brains. Apart from a lower oscillation frequency in neonates, the most obvious difference between the two developmental stages is the existence of small- and large-amplitude neuronal sodium transients at P14-16 only.

Effect of a general inhibition of sodium-dependent glutamate transport

To study the contribution of GLAST versus GLT-1 to cellular sodium oscillations and network function, we first applied the non-transported, competitive inhibitor TFB-TBOA (1 μM), which blocks both transporter subtypes (Shimamoto et al., 1998; Tsukada et al., 2005; Bernardinelli et al., 2008). Perfusion of slices taken from P14-16 animals with TFB-TBOA for 15 minutes during recurrent network activity had a massive impact on sodium signaling (N=3). Within 2-3 minutes, the frequency of neuronal sodium oscillations increased, while at the same time recovery slowed down, resulting in a rapid build-up of neuronal sodium concentration (Fig. 4A1). Subsequently, the amplitude of individual sodium increases went down, until during phase 2, 14 out of 108 neurons did not show detectable signals anymore, while the frequency and amplitude of the remaining signals displayed massive reduction (Fig. 3A1, B1; 4A1). Finally, sodium loading slowed down and neuronal sodium concentration reached 22.3 ± 0.7 mM above the initial baseline (n=108 cells) (Fig. 3C1, 4A1). The effects of TFB-TBOA were not reversible. 15-20 minutes after onset of TFB-TBOA perfusion (which means at the very end of its perfusion or during the wash-out period), most neurons experienced a rapid loss of dye as evident from a steep drop of the fluorescence emission at both 340 and 380 nm, indicating loss of membrane integrity (illustrated by two-photon microscopy as shown in Fig. 4B1).

In astrocytes, the frequency of sodium signals changed in parallel to neuronal oscillations, while their peak amplitude decreased (Figs. 3A1, B1, 4A1). Astrocytes' sodium oscillations ceased completely around the time when neuronal sodium loading neared its maximum (Fig. 4A1). In contrast to neurons, however, overall sodium loading of astrocytes was moderate, reaching 3.9 ± 0.6 mM in phase 2 (n=44 cells) (Fig. 3C1). At the same time, dye loss from astrocyte cell bodies was not apparent (Fig. 4B1).

In tissue slices derived from neonate animals (N=3), TFB-TBOA exerted overall similar effects, which albeit developed more quickly than at P14-16 (Figs. 4A2). This included a cessation of network sodium oscillations, accompanied by a rapid and strong increase of the neuronal baseline sodium by 36.2 ± 1.0 mM (n=62 cells) (Figs. 3A2, C2). Maximum projection images of z-stacks taken at a two-photon microscope revealed a loss of dye from neuronal cell bodies (Fig. 4B2). In astrocytes (n=74 cells), only minor changes in sodium (Fig. 3C2, 4A2) were observed, and most cells maintained their membrane integrity (Fig. 4B2), while only a minority of cells (6 out of 74 cells) showed a

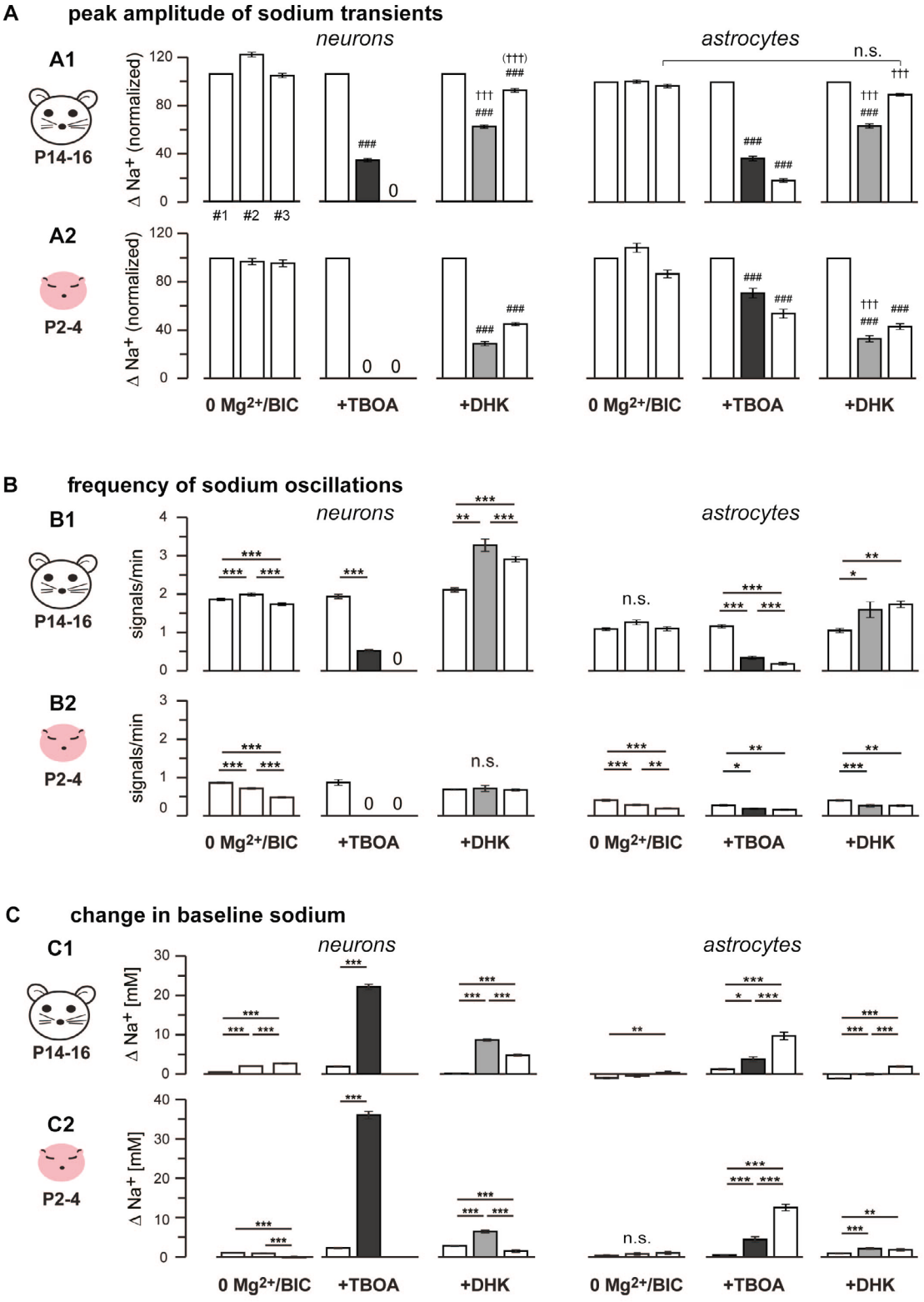

Figure 3. *Properties of network sodium oscillations. Groups of bar graphs show results obtained by analysis of phases 1, 2 and 3, respectively (cf. Fig. 1) in neurons (left half) and astrocytes (right half). Small and large neuronal sodium transients were pooled. In all experiments, 0Mg²⁺/BIC was continuously applied throughout phase 1, 2 and 3 (#1, #2, #3). Filled bars highlight results from phase 2, during which the indicated additional substance was present (+TFB-TBOA (dark grey); +DHK (light grey)). A) displays changes in the sodium peak amplitudes in phase 2 and 3, normalized to phase 1 of P14-16 (A1) and neonatal (A2) slices. Asterisks indicate p-values of differences between different phases, rhombs reflect p-values of differences to time-matched control conditions (0Mg²⁺/BIC), crosses reflect p-values of differences between time-matched DHK and TFB-TBOA conditions (*≡ p<0.05; **≡ p<0.01; ***/###/††† ≡ p<0.001). B) Frequency of sodium transients per minute for P14-16 (B1) and neonatal (B2) neurons and astrocytes. C) Change of the sodium baseline concentration as compared to ACSF (phase 0).*

 doi:10.20388/omp2017.003.0048

loss of dye after washout of TFB-TBOA.

These results thus confirm the expected critical role of sodium-dependent glutamate transport for neural network activity and for maintenance of neuronal sodium homeostasis in early postnatal brain. Our data furthermore demonstrate that this also applies for very early postnatal development, during which blockage of glutamate transport led to rapid loss of recurrent electrical activity and a partial breakdown of the sodium gradient, accompanied by rapid loss of membrane integrity. Astrocytes displayed an astonishing resistance to this manipulation at both developmental stages, maintaining a low baseline sodium concentration despite excessive neuronal damage.

Effect of the GLT-1 blocker DHK

Earlier studies have revealed that GLAST is the predominant transporter subtype in the neonate hippocampus, while GLT-1 is upregulated during the second week of postnatal development (Rothstein et al., 1994; Furuta et al., 1997; Ullensvang et al., 1997; Schreiner et al., 2014). To study the specific functional role of GLT-1 at both developmental stages, we employed dihydrokainate (DHK, 300 μM), a specific antagonist of this transporter (Shimamoto et al., 1998; Chatton et al., 2001).

In slices derived from P14-16 animals (N=3), application of DHK to block GLT-1 exerted similar, but overall much milder effects as compared to blocking both transporter subtypes with TFB-TBOA (Fig. 5A1). The peak amplitude of neuronal sodium transients was reduced by about 40% and baseline concentration of neurons only rose by about 10 mM (8.7 ± 0.2 mM; n=116 neurons; Figs. 3A1, C1). In stark contrast to TFB-TBOA, oscillations persisted, however with significantly increased frequency (Figs. 3B1, 5A1). During washout of DHK, a partial recovery towards baseline levels and initial network activity was observed (Figs. 3, 5A1). In astrocytes, only minor changes in baseline sodium were seen (n=46 cells), while – as observed in neurons - the amplitude of sodium transients dropped with increasing oscillation frequency (Figs. 3, 5A1). Maximum projection images obtained using two-photon microscopy showed no apparent loss of dye from neither neurons nor astrocytes (Fig. 5B1).

In neonatal animals (N=4), DHK exposure had a similar effect as in P14-16 tissue considering the peak amplitude of neuronal sodium signals and sodium baseline (n= 136 cells) (Figs. 3A2, C2; 5A2). In contrast to the situation in two-week-old animals, DHK, however, had no significant effect on the frequency of neuronal oscillations (Fig. 3B2). In astrocytes, DHK caused a drop in the amplitude of sodium signals, resulting in a decreased number of detectable sodium transients, as evident from the drop in the frequency of astrocyte oscillations (n=85 cells) (Fig. 3A2, B2, C2). Compared to the strong effect of TFB-TBOA in neonates, DHK did not result in a major loss of dye from the cells, albeit some swelling of neuronal cell bodies was observed (Fig. 5B2).

Taken together, these data show that specific inhibition of GLT-1 with DHK affected neural signaling and neuronal sodium homeostasis in both two-week-old and neonate animals. Effects are, however, much more prominent in animals at P14-16, which also experience a strong increase in oscillation frequency upon block of GLT-1 that is not observed in neonates.

Discussion

In the present study, we demonstrate that neurons and astrocytes in hippocampal tissue slices derived from both two-week-old and early neonatal mouse brain undergo persistent network-wide somatic sodium oscillations upon removal of external magnesium and application of bicuculline. Functional high-affinity glutamate transport is critically required for network activity as well as for the regulation of neuronal sodium and the cellular integrity of neurons during both developmental stages. Our study also suggests a developmental switch in the functional relevance of the two transporter subtypes for maintenance of sodium homeostasis and recurrent network activity: while GLT-1 seems to be more prominent at P14-16, GLAST predominates at P2-4.

Relevance of sodium-dependent glutamate uptake for network activity and cellular sodium homeostasis

Our work shows that dis-inhibition induces synchronized sodium oscillations in essentially the entire population of CA1 pyramidal neurons and astrocytes in the CA1 stratum radiatum of mouse hippocampus, confirming our recent observations (Karus et al., 2015). While we focused on global network signaling and detection of somatic sodium transients, it was demonstrated earlier that with local stimulation of afferent fibres, sodium signals are largely restricted to their site of influx - that is close to activated synapses (Langer & Rose, 2009). Sodium is a highly mobile, essentially unbuffered ion, but it is probably safe to assume that changes in sodium concentration will be significantly larger in cellular microdomains - that is in fine perisynaptic astrocyte processes and/or spiny dendrites - as compared to cell bodies.

Astrocytes take up the majority of extracellular glutamate and thereby shape synaptic transmission at glutamatergic synapses (Danbolt, 2001). In addition, glutamate uptake protects the brain from glutamate-induced over-excitation and excitotoxic damage (Maragakis et al., 2004). High-affinity glutamate transporters couple influx of three sodium ions to the uptake of glutamate (Danbolt, 2001; Schousboe et al., 2004) and represent a major pathway for activity-dependent sodium influx into astrocytes (Kirischuk et al., 2016; Rose et al., 2016c). Consequently, the non-transported competitive inhibitor TBOA as well as its more potent version TFB-TBOA (Shimamoto et al., 1998; Tsukada et al., 2005; Bernardinelli et al., 2008), which have a similar affinity for all transporter subtypes, virtually eliminate synaptically-induced sodium transients in hippocampal astrocytes (Langer et al., 2009).

When employed in hippocampal tissue slices, (TFB-) TBOA induces an immediate increase in the extracellular glutamate concentration, followed by a substantial

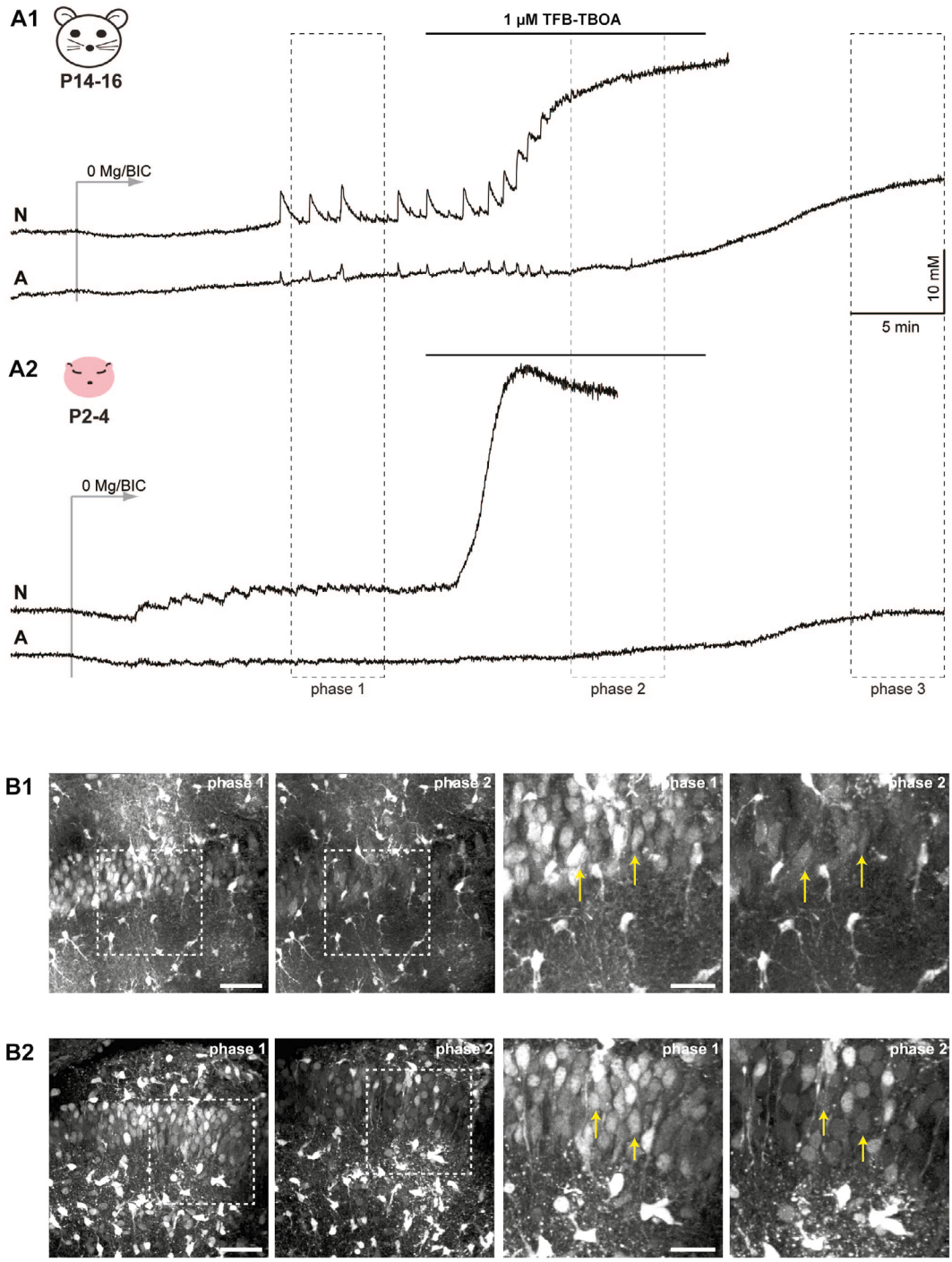

Figure 4. *Effects of blocking GLAST and GLT-1 by TFB-TBOA. A) Effect of TFB-TBOA on sodium oscillations and sodium homeostasis in P14-16 (A1) and neonatal slices (A2). B) Maximum projection images of z-stacks taken at a two-photon microscope in phase 1 (0 Mg^{2+}/BIC) and 2 (TFB-TBOA) at two different magnifications in P14-16 (B1) and neonatal slices (B2). Boxes indicate regions shown enlarged on the right. Arrows point to cells that experienced significant dye loss in phase 2. Scale bars: 50 µm (left) and 25 µm (right).*

depolarization of neurons related to the activation of glutamate receptors (e. g. Jabaudon et al., 1999). This is accompanied by rapid and irreversible sodium loading of neurons, which even occurs "at rest", without additional synaptic stimulation (Langer et al., 2009). Hippocampal astrocytes, in the contrary, only show minor and slowly developing changes in their baseline sodium concentration during the application of (TFB-)TBOA, indicating that - with glutamate uptake blocked - the rising extracellular glutamate concentration does not activate sodium-permeable ion channels such as e. g. ionotropic glutamate receptors in these cells (Langer et al., 2009; Langer et al., 2017).

During epileptiform activity, a similar phenomenon occurs: upon inhibition of glutamate uptake by TFB-TBOA, neurons quickly load with sodium, while

 doi:10.20388/omp2017.003.0048

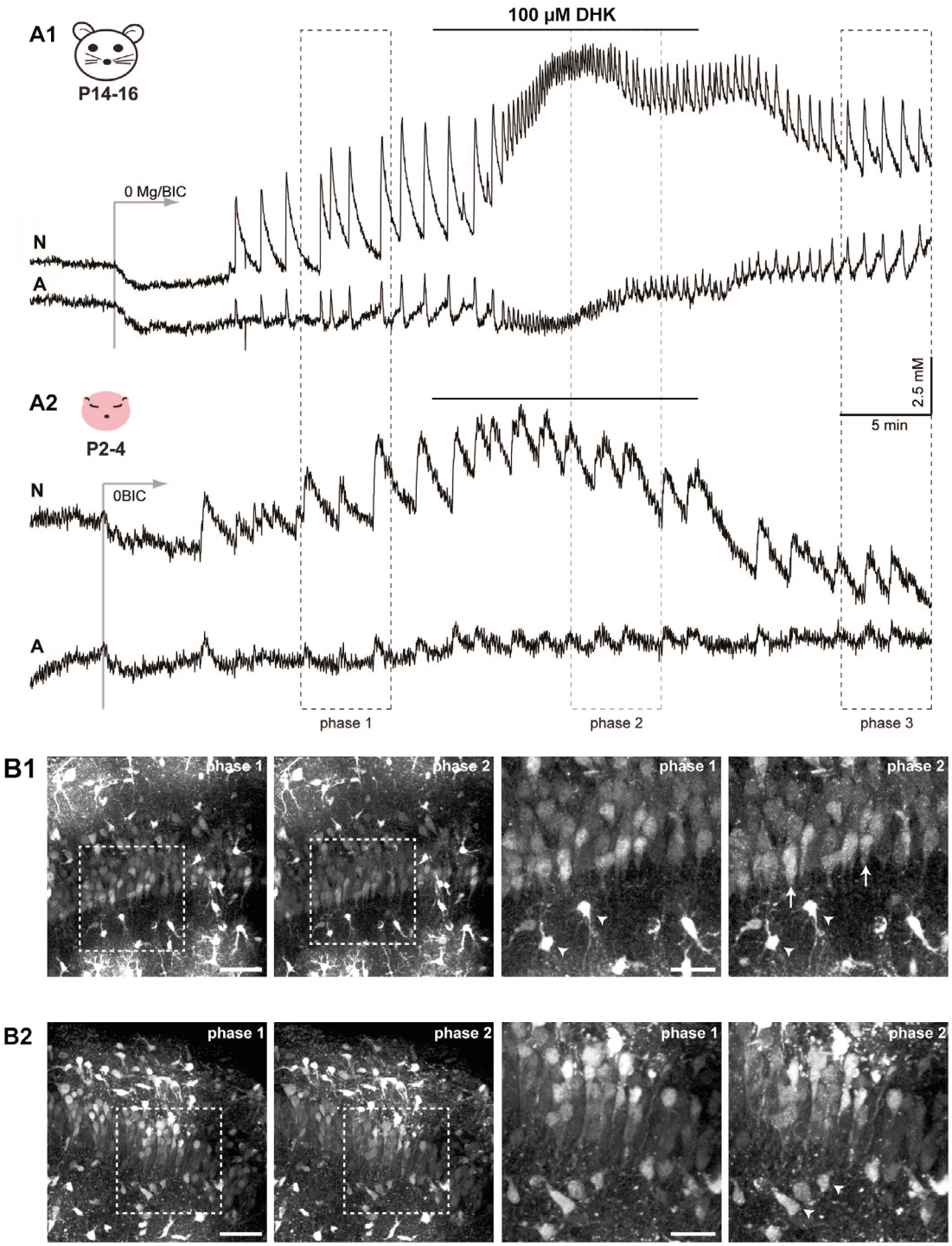

Figure 5. *Effects of blocking GLT-1 by DHK. A) Effect of DHK on sodium oscillations and sodium homeostasis in P14-16 (A1) and neonatal slices (A2). B) Maximum projection images of z-stacks taken at a two-photon microscope in phase 1 (0 Mg^{2+}/BIC) and 2 (DHK) at two different magnifications in P14-16 (B1) and neonatal slices (B2). Boxes indicate regions shown enlarged on the right. Cells did not experience significant dye loss in phase 2, albeit some swelling of cell bodies is apparent. Scale bars: 50 µm (left) and 25 µm (right).*

astrocytes are only affected moderately (Karus et al., 2015a), an observation confirmed in the present study. Neurons displayed no ability to recover from this sodium load and showed clear signs of cellular damage within a few minutes after reaching their maximum sodium concentrations. This was paralleled by a change in the pattern of electrical activity, at first resulting in an increase in discharge frequency, followed by cessation of activity (Karus et al., 2015a). The previous, as well as the present study showed that neuronal sodium oscillations thus mirrors electrical behaviour. The strong sodium loading of neurons in the presence of glutamate transport blockers is thus probably due to non-linear amplification of excitability and sodium entry. Indeed, fatal sodium loading of neurons could be limited by blocking sodium influx through ionotropic glutamate receptors (AMPA/

NMDA receptor channels), which, at the same time, eliminated epileptiform activity (Karus et al., 2015a).

Altogether, these experiments thus emphasize the essential role of glutamate transport for maintenance of electrical activity, sodium homeostasis and function of neurons by protecting them from glutamate-mediated excitotoxicity and/or swelling-mediated rapid cell death (Choi et al., 1990; Rothstein et al., 1996; Rungta et al., 2015). Hippocampal astrocytes, on the other hand, are astonishingly resistant to "excitotoxic" conditions induced by blocking glutamate uptake. Even while extracellular glutamate accumulates and electrical activity accelerates at first, astrocytes do not show a strong increase in their intracellular sodium concentration, indicating that the absence of functional glutamate uptake protects them from sodium overload.

Functional relevance of GLT-1 and GLAST in two-week-old vs. neonate brains

Astrocytes in the rodent hippocampus express two types of glutamate transporters, GLAST and GLT-1 (Storck et al., 1992; Chaudhry et al., 1995; Gegelashvili et al., 1998; Lehre et al., 1998). GLT-1 is the isoform considered to be of major relevance for glutamate clearance in the juvenile and mature brain, and mice lacking this isoform suffer from fatal epileptic seizures and die after a few weeks only (Tanaka et al., 1997). Notably, while it is established that astrocytes take up the majority of glutamate, GLT-1 is also expressed on presynaptic terminals (Mennerick et al., 1998; Zhou et al., 2014).

In the present study, we show that, consistent with the critical role of GLT-1 for glutamate homeostasis and network function in postnatal brain, its inhibition by DHK causes a strong sodium loading of neurons as well as an increase in the frequency of network oscillations. Compared to TFB-TBOA, the effects of DHK were relatively mild. Importantly, rapid loss of intracellular dye, indicating loss of membrane integrity, was not observed in the time frame of the experiments. This indicates that GLAST contributes to glutamate clearance at P14-16 and can partly compensate a lack of GLT-1 function, thereby helping to protect neurons from excitotoxicity. On the other hand, GLAST-knock-out mice show only a mild phenotype, that is mainly restricted to specific motor deficits and increased susceptibility to edema formation after injury (Watase et al., 1998). Glial GLT-1 and/or other glutamate transporter isoforms expressed by neurons are thus largely able to compensate a lack of GLAST activity.

Glutamatergic synapses and network formation only fully develop in the first few weeks after birth (Ben-Ari, 2001). The formation of glutamatergic synapses is accompanied by the proliferation, differentiation and maturation of the astrocyte population, which mainly takes place in the first and second postnatal week (Ullian et al., 2004). During their maturation, the properties of astrocytes change dramatically and they switch from cells expressing voltage-dependent conductances to classic "passive" astrocytes (Kressin et al., 1995; Bordey et al., 1997; Zhou et al., 2006; Kafitz et al., 2008). These changes in ion channel expression of astrocytes are paralleled by changes in glutamate uptake. While there is a general increase in glutamate transporter expression from birth to adulthood (Furuta et al., 1997; Kugler et al., 2004), there is also a switch in isoform expression. Thus, in neonates, GLAST is the predominant isoform, while GLT-1 is barely detectable (Shibata et al., 1997; Raponi et al., 2007; Schreiner et al., 2014; Hanson et al., 2015; Rose et al., 2016d).

The established dominance of GLAST over GLT-1 explains the relatively weak effect of DHK on epileptiform activity and sodium oscillations in neonates observed in the present study. Still, even at this very young age, GLAST activity can apparently not fully compensate for a lack of GLT-1. Indeed, while inhibition of GLT-1 by DHK was not accompanied by major sodium loading and an increase in oscillation frequency in neonates, it still caused a detectable increase in neuronal baseline sodium concentration and a decrease in the peak amplitude of neuronal sodium transients.

In summary, our results show that the functional relevance of GLAST and GLT-1 for maintenance of sodium homeostasis and recurrent network activity changes during early postnatal brain development: while GLT-1 seems to be more prominent at P14-16, GLAST predominates at P2-4. Nonetheless, the data also clearly indicate that both transporters have a functional role and contribute to the clearance of glutamate from the extracellular space during recurrent network activity in the P14-16 as well as in the neonatal brain. Lack of GLT-1 activity can thus be partially compensated by GLAST, an observation which holds true even in the two-week-old brain, where GLAST is considered to be functionally weak and GLT-1 regarded as the major glutamate uptake pathway. Furthermore, lack of GLT-1 also visibly disturbs glutamate clearance in the neonate and cannot be fully compensated by GLAST activity, although the latter represents the major transporter subtype expressed at this age.

Acknowledgements

We thank Simone Durry and Claudia Roderigo for excellent technical assistance and Joel E. Nelson, Institute of Neurobiology, for critical comments on the manuscript. This study was supported by the Special Priority Program 1757 "Glial Heterogeneity" of the DFG (German Research Foundation; Ro 2327/8-1, 8-2).

References

ARAQUE A., CARMIGNOTO G., HAYDON P.G., OLIET S.H., ROBITAILLE R. & VOLTERRA A. (2014): Gliotransmitters Travel in Time and Space. Neuron. 81,728-739.

ATTWELL D., BUCHAN A.M., CHARPAK S., LAURITZEN M., MACVICAR B.A. & NEWMAN E.A. (2010): Glial and neuronal control of brain blood flow. Nature. 468,232-243.

 doi:10.20388/omp2017.003.0048

BAK L.K., SCHOUSBOE A. & WAAGEPETERSEN H.S. (2006): The glutamate/GABA-glutamine cycle: aspects of transport, neurotransmitter homeostasis and ammonia transfer. J Neurochem. 98,641-653.

BEN-ARI Y. (2001): Developing networks play a similar melody. Trends Neurosci. 24,353-360.

BENNAY M., LANGER J., MEIER S.D., KAFITZ K.W. & ROSE C.R. (2008): Sodium signals in cerebellar Purkinje neurons and Bergmann glial cells evoked by glutamatergic synaptic transmission. Glia. 56,1138-1149.

BERNARDINELLI Y. & CHATTON J.Y. (2008): Differential effects of glutamate transporter inhibitors on the global electrophysiological response of astrocytes to neuronal stimulation. Brain Res. 1240,47-53.

BORDEY A. & SONTHEIMER H. (1997): Postnatal development of ionic currents in rat hippocampal astrocytes in situ. J Neurophysiol. 78,461-477.

BOSCIA F., BEGUM G., PIGNATARO G., SIRABELLA R., CUOMO O., CASAMASSA A., SUN D. & ANNUNZIATO L. (2016): Glial Na(+) -dependent ion transporters in pathophysiological conditions. Glia. 64,1677-1697.

CHATTON J.Y., MAGISTRETTI P.J. & BARROS L.F. (2016): Sodium signaling and astrocyte energy metabolism. Glia. 64,1667-1676.

CHATTON J.Y., SHIMAMOTO K. & MAGISTRETTI P.J. (2001): Effects of glial glutamate transporter inhibitors on intracellular Na^+ in mouse astrocytes. Brain Res. 893,46-52.

CHAUDHRY F.A., LEHRE K.P., VAN LOOKEREN CAMPAGNE M., OTTERSEN O.P., DANBOLT N.C. & STORM-MATHISEN J. (1995): Glutamate transporters in glial plasma membranes: highly differentiated localizations revealed by quantitative ultrastructural immunocytochemistry. Neuron. 15,711-720.

CHOI D.W. & ROTHMAN S.M. (1990): The role of glutamate neurotoxicity in hypoxic-ischemic neuronal death. Annu Rev Neurosci. 13,171-182.

DANBOLT N.C. (2001): Glutamate uptake. Prog Neurobiol. 65,1-105.

EDWARDS F.A., KONNERTH A., SAKMANN B. & TAKAHASHI T. (1989): A thin slice preparation for patch clamp recordings from neurones of the mammalian central nervous system. Pflugers Arch. 414,600-612.

FELLIN T., GOMEZ-GONZALO M., GOBBO S., CARMIGNOTO G. & HAYDON P.G. (2006): Astrocytic glutamate is not necessary for the generation of epileptiform neuronal activity in hippocampal slices. J Neurosci. 26,9312-9322.

FURUTA A., ROTHSTEIN J.D. & MARTIN L.J. (1997): Glutamate transporter protein subtypes are expressed differentially during rat CNS development. J Neurosci. 17,8363-8375.

GEGELASHVILI G. & SCHOUSBOE A. (1998): Cellular distribution and kinetic properties of high-affinity glutamate transporters. Brain Res Bull. 45,233-238.

GERKAU N.J., RAKERS C., PETZOLD G.C. & ROSE C.R. (2017): Differential effects of energy deprivation on intracellular sodium homeostasis in neurons and astrocytes. J Neurosci Res.10.1002/jnr.23995.

HANSON E., ARMBRUSTER M., CANTU D., ANDRESEN L., TAYLOR A., DANBOLT N.C. & DULLA C.G. (2015): Astrocytic glutamate uptake is slow and does not limit neuronal NMDA receptor activation in the neonatal neocortex. Glia. 63,1784-1796.

JABAUDON D., SHIMAMOTO K., YASUDA-KAMATANI Y., SCANZIANI M., GAHWILER B.H. & GERBER U. (1999): Inhibition of uptake unmasks rapid extracellular turnover of glutamate of nonvesicular origin. Proc Natl Acad Sci U S A. 96,8733-8738.

KAFITZ K.W., MEIER S.D., STEPHAN J. & ROSE C.R. (2008): Developmental profile and properties of sulforhodamine 101-labeled glial cells in acute brain slices of rat hippocampus. J Neurosci Methods. 169,84-92.

KARUS C., MONDRAGAO M.A., ZIEMENS D. & ROSE C.R. (2015a): Astrocytes restrict discharge duration and neuronal sodium loads during recurrent network activity. Glia. 63,936-957.

KARUS C., ZIEMENS D. & ROSE C.R. (2015b): Lactate rescues neuronal sodium homeostasis during impaired energy metabolism. Channels (Austin). 9,200-208.

KIRISCHUK S., HEJA L., KARDOS J. & BILLUPS B. (2016): Astrocyte sodium signaling and the regulation of neurotransmission. Glia. 64,1655-1666.

KIRISCHUK S., KETTENMANN H. & VERKHRATSKY A. (2007): Membrane currents and cytoplasmic sodium transients generated by glutamate transport in Bergmann glial cells. Pflugers Arch. 454,245-252.

KIRISCHUK S., PARPURA V. & VERKHRATSKY A. (2012): Sodium dynamics: another key to astroglial excitability? Trends Neurosci. 35,497-506.

KRESSIN K., KUPRIJANOVA E., JABS R., SEIFERT G. & STEINHAUSER C. (1995): Developmental regulation of Na^+ and K^+ conductances in glial cells of mouse hippocampal brain slices. Glia. 15,173-187.

KUGLER P. & SCHLEYER V. (2004): Developmental expression of glutamate transporters and glutamate dehydrogenase in astrocytes of the postnatal rat hippocampus. Hippocampus. 14,975-985.

LANGER J., GERKAU N.J., DEROUICHE A., KLEINHANS C., MOSHREFI-RAVASDJANI B., FREDRICH M., KAFITZ K.W., SEIFERT G., STEINHAUSER C. & ROSE C.R. (2017): Rapid sodium signaling couples glutamate uptake to breakdown of ATP in perivascular astrocyte endfeet. Glia. 65,293-308.

LANGER J. & ROSE C.R. (2009): Synaptically induced sodium signals in hippocampal astrocytes in situ. J Physiol. 587,5859-5877.

LANGER J., STEPHAN J., THEIS M. & ROSE C.R. (2012): Gap junctions mediate intercellular spread of sodium between hippocampal astrocytes in situ. Glia. 60,239-252.

LEHRE K.P. & DANBOLT N.C. (1998): The number of glutamate transporter subtype molecules at glutamatergic synapses: chemical and stereological

quantification in young adult rat brain. J Neurosci. 18,8751-8757.
MARAGAKIS N.J. & ROTHSTEIN J.D. (2004): Glutamate transporters: animal models to neurologic disease. Neurobiol Dis. 15,461-473.
MEIER S.D., KOVALCHUK Y. & ROSE C.R. (2006): Properties of the new fluorescent Na^+ indicator CoroNa Green: comparison with SBFI and confocal Na^+ imaging. J Neurosci Methods. 155,251-259.
MENNERICK S., DHOND R.P., BENZ A., XU W., ROTHSTEIN J.D., DANBOLT N.C., ISENBERG K.E. & ZORUMSKI C.F. (1998): Neuronal expression of the glutamate transporter GLT-1 in hippocampal microcultures. J Neurosci. 18,4490-4499.
NEDERGAARD M. & VERKHRATSKY A. (2012): Artifact versus reality-How astrocytes contribute to synaptic events. Glia. 60,1013-1023.
NIMMERJAHN A., KIRCHHOFF F., KERR J.N. & HELMCHEN F. (2004): Sulforhodamine 101 as a specific marker of astroglia in the neocortex in vivo. Nat Methods. 1,31-37.
PARPURA V., SEKLER I. & FERN R. (2016): Plasmalemmal and mitochondrial Na -Ca exchange in neuroglia. Glia. 64,1646-1654.
PELLERIN L. & MAGISTRETTI P.J. (2012): Sweet sixteen for ANLS. J Cereb Blood Flow Metab. 32,1152-1166.
RAPONI E., AGENES F., DELPHIN C., ASSARD N., BAUDIER J., LEGRAVEREND C. & DELOULME J.C. (2007): S100B expression defines a state in which GFAP-expressing cells lose their neural stem cell potential and acquire a more mature developmental stage. Glia. 55,165-177.
ROSE C.R. & CHATTON J.Y. (2016a): Astrocyte sodium signaling and neuro-metabolic coupling in the brain. Neuroscience. 323,121-134.
ROSE C.R. & KARUS C. (2013): Two sides of the same coin: sodium homeostasis and signaling in astrocytes under physiological and pathophysiological conditions. Glia. 61,1191-1205.
ROSE C.R. & VERKHRATSKY A. (2016b): Glial ionic excitability: The role for sodium. Glia. 64,1609-1610.
ROSE C.R. & VERKHRATSKY A. (2016c): Principles of sodium homeostasis and sodium signalling in astroglia. Glia. 64,1611-1627.
ROSE C.R., ZIEMENS D., UNTIET V. & FAHLKE C. (2016d): Molecular and cellular physiology of sodium-dependent glutamate transporters. Brain Res Bull.10.1016/j.brainresbull.2016.1012.1013.
ROTHSTEIN J.D., DYKES-HOBERG M., PARDO C.A., BRISTOL L.A., JIN L., KUNCL R.W., KANAI Y., HEDIGER M.A., WANG Y., SCHIELKE J.P. & WELTY D.F. (1996): Knockout of glutamate transporters reveals a major role for astroglial transport in excitotoxicity and clearance of glutamate. Neuron. 16,675-686.
ROTHSTEIN J.D., MARTIN L., LEVEY A.I., DYKES-HOBERG M., JIN L., WU D., NASH N. & KUNCL R.W. (1994): Localization of neuronal and glial glutamate transporters. Neuron. 13,713-725.
ROUACH N., KOULAKOFF A., ABUDARA V., WILLECKE K. & GIAUME C. (2008): Astroglial metabolic networks sustain hippocampal synaptic transmission. Science. 322,1551-1555.
RUNGTA R.L., CHOI H.B., TYSON J.R., MALIK A., DISSING-OLESEN L., LIN P.J., CAIN S.M., CULLIS P.R., SNUTCH T.P. & MACVICAR B.A. (2015): The cellular mechanisms of neuronal swelling underlying cytotoxic edema. Cell. 161,610-621.
RUSAKOV D.A. (2015): Disentangling calcium-driven astrocyte physiology. Nat Rev Neurosci. 16,226-233.
SCHOUSBOE A., SARUP A., BAK L.K., WAAGEPETERSEN H.S. & LARSSON O.M. (2004): Role of astrocytic transport processes in glutamatergic and GABAergic neurotransmission. Neurochem Int. 45,521-527.
SCHREINER A.E., DURRY S., AIDA T., STOCK M.C., RÜTHER U., TANAKA K., ROSE C.R. & KAFITZ K.W. (2014): Laminar and subcellular heterogeneity of GLAST and GLT-1 immunoreactivity in the developing postnatal mouse hippocampus. Journal of Comparative Neurology. 522,204-224.
SHIBATA T., YAMADA K., WATANABE M., IKENAKA K., WADA K., TANAKA K. & INOUE Y. (1997): Glutamate transporter GLAST is expressed in the radial glia-astrocyte lineage of developing mouse spinal cord. J Neurosci. 17,9212-9219.
SHIMAMOTO K., LEBRUN B., YASUDA-KAMATANI Y., SAKAITANI M., SHIGERI Y., YUMOTO N. & NAKAJIMA T. (1998): DL-threo-beta-benzyloxyaspartate, a potent blocker of excitatory amino acid transporters. Mol Pharmacol. 53,195-201.
SOMJEN G.G. (2002): Ion regulation in the brain: implications for pathophysiology. Neuroscientist. 8,254-267.
STORCK T., SCHULTE S., HOFMANN K. & STOFFEL W. (1992): Structure, expression, and functional analysis of a Na(+)-dependent glutamate/aspartate transporter from rat brain. Proc Natl Acad Sci U S A. 89,10955-10959.
TANAKA K., WATASE K., MANABE T., YAMADA K., WATANABE M., TAKAHASHI K., IWAMA H., NISHIKAWA T., ICHIHARA N., KIKUCHI T., OKUYAMA S., KAWASHIMA N., HORI S., TAKIMOTO M. & WADA K. (1997): Epilepsy and exacerbation of brain injury in mice lacking the glutamate transporter GLT-1. Science. 276,1699-1702.
TSUKADA S., IINO M., TAKAYASU Y., SHIMAMOTO K. & OZAWA S. (2005): Effects of a novel glutamate transporter blocker, (2S, 3S)-3-[3-[4-(trifluoromethyl) benzoylamino]benzyloxy]aspartate (TFB-TBOA), on activities of hippocampal neurons. Neuropharmacology. 48,479-491.
ULLENSVANG K., LEHRE K.P., STORM-MATHISEN J. & DANBOLT N.C. (1997): Differential developmental expression of the two rat brain glutamate transporter proteins GLAST and GLT. Eur J Neurosci. 9,1646-1655.
ULLIAN E.M., CHRISTOPHERSON K.S. & BARRES B.A. (2004): Role for glia in synaptogenesis. Glia. 47,209-216.
UWECHUE N.M., MARX M.C., CHEVY Q. & BILLUPS

B. (2012): Activation of glutamate transport evokes rapid glutamine release from perisynaptic astrocytes. J Physiol. 590,2317-2331.

WATASE K., HASHIMOTO K., KANO M., YAMADA K., WATANABE M., INOUE Y., OKUYAMA S., SAKAGAWA T., OGAWA S.-I., KAWASHIMA N., HORI S., TAKIMOTO M., WADA K. & TANAKA K. (1998): Motor discoordination and increased susceptibility to cerebellar injury in GLAST mutant mice. Eur J Neurosci. 10,976-988.

ZHOU M., SCHOOLS G.P. & KIMELBERG H.K. (2006): Development of GLAST(+) astrocytes and NG2(+) glia in rat hippocampus CA1: mature astrocytes are electrophysiologically passive. J Neurophysiol. 95,134-143.

ZHOU Y. & DANBOLT N.C. (2014): Glutamate as a neurotransmitter in the healthy brain. J Neural Transm (Vienna). 121,799-817.